High-pressure phase transitions of solid HF, HCl, and HBr: An *ab initio* evolutionary study

Lijun Zhang, Yanchao Wang, Xinxin Zhang, and Yanming Ma*
State Key Laboratory of Superhard Materials, Jilin University, Changchun 130012, People's Republic of China
(Received 4 April 2010; revised manuscript received 24 June 2010; published 16 July 2010)

Using *ab initio* evolutionary methodology for structure predictions, we investigated the high-pressure phase diagram for solid-state HF, HCl, and HBr at zero temperature. The ambient-pressure chain-type $Cmc2_1$ structure and sequent high-pressure symmetric hydrogen-bonded *Cmcm* structure were successfully reproduced by structural simulations with the only known information of chemical compositions. We have also presented insight into the underlying mechanism of hydrogen-bond symmetrization at the $Cmc2_1 \rightarrow Cmcm$ transformation, by analysis of electron localization functions, potential wells, and zone-center phonons with pressure. At higher pressures, it was predicted that HF transforms from the *Cmcm* phase to another chain-type *Pnma* structure at ~143 GPa while the post-*Cmcm* phase of HCl and HBr adopts an intriguing triclinic $P\bar{1}$ structure at above 108 GPa and 59 GPa, respectively, which consists of nearly planar squares resembling the ambient phase of HI. The newly predicted high-pressure phases of these halides all contain symmetric hydrogen bonds and satisfy lattice dynamical stability. As for the earlier proposed dissociation of HBr, we found that this can only occur at rather high pressures (above 120 GPa) with the formation of monatomic Br and solid H_2.

DOI: 10.1103/PhysRevB.82.014108 PACS number(s): 61.50.Ks, 61.50.Ah, 71.15.Nc, 63.20.D−

I. INTRODUCTION

The simple molecular solids formed by diatomic molecules, hydrogen halides H*X* (*X*=F, Cl, Br, and I), possess strong to modest hydrogen bonds and have attracted much attention for decades. The systematic studies on this family are greatly helpful for the understanding of intriguing natures of hydrogen bonds. It is well accepted that pressure can efficiently revise the bonding properties of materials, including hydrogen bonds containing systems.[1–3] It is thus expected that upon compression the abundant bonding changes in hydrogen halides could occur and eventually result in structural phase transitions. In addition, the potential high-pressure metallization in these hydrides might shed light on the understanding of metallic hydrogen.[4,5]

At ambient pressure, the distinct strength of hydrogen bonds results in the formation of different crystal structures in hydrogen halides. Hydrogen fluoride (HF) with the largest electronegativity of fluorine, having the strongest hydrogen bonds, crystallizes in an orthorhombic $Cmc2_1$ structure consisting of planar zigzag chains of HF molecules,[6] as shown in Fig. 1. In addition to covalent bonds within molecules, each H atom forms hydrogen bond with the second-nearest F atom along the chain. The molecular chains are arranged along the *c* axis and aligned in the planes parallel to the *bc* plane, and between neighboring chains the weak van der Waals interactions exist. Unlike HF, the hydrogen bonds for the heavier halogen hydrides, H*X* (*X*=Cl, Br, and I), are much weaker. This gives rise to orientationally disordered molecular phases (phases I and II) at high temperatures.[7–9] At very low temperatures, hydrogen chloride (HCl) and hydrogen bromide (HBr) adopt the ordered phase III, which is structurally isomorphic to the $Cmc2_1$ phase of HF.[9,10] For hydrogen iodide (HI), the molecular ordering appears in a different way at low temperatures, which occurs in a complex triclinic $P\bar{1}$ structure, consisting of distorted diamonds (almost squares), rather than chains.[9,11]

Raman-scattering measurements for HF up to 12 GPa showed that there was a dramatic change at ~6 GPa in the librational spectra accompanied by the disappearance of the translational and stretching modes.[12] These features were suggested as a sign of transformation into a symmetric hydrogen-bonded phase (space group *Cmcm*), in which protons relocate to exactly halfway between two F atoms (with equal length of dashed lines and stick bonds in Fig. 1), similar to the symmetric phase X of ice.[13] However, the authors failed to observe this transition in the high-pressure Brillouin scattering experiments.[14] For HCl and HBr, at room temperature and low pressures the transition from the disordered phase I to the ordered phase III ($Cmc2_1$) was experimentally determined.[15–18] With increasing pressure, phase III was observed to further transform to phase IV with symmetric hydrogen bonds (the same *Cmcm* phase as proposed for HF) at ~32 GPa (Ref. 19) [39 GPa (Ref. 17)] for HBr and 51 GPa for HCl (Ref. 16) [56 GPa for DCl (Ref. 18)], by evidence of a strong redshift of the stretching mode that eventually disappears at the transition. Additionally, Katoh *et al.*[16,17] suggested that the phase IV of HBr is instable and decompose shortly after the transition to form Br_2 molecules, judged by the appearance of Br_2 molecular Raman peaks. A subsequent *ab initio* molecular-dynamics (AIMD) study on HBr at high

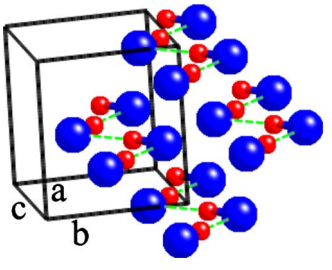

FIG. 1. (Color online) Crystal structure of the ordered $Cmc2_1$ phase at ambient pressure for HF, HCl, and HBr. The halogen atoms are marked as larger spheres and hydrogen as smaller ones. The hydrogen bonds are depicted as green dashed lines. It can also be viewed as the *Cmcm* structure (phase IV) if the hydrogen atoms are located at the midpoint of two halogens within the chain.

TABLE I. Optimized structural parameters (a, b, c, and V), covalent-bond length ($d_{H\text{-}X}$), distance between nearest halogens ($d_{X\text{-}X}$), and bond angle of covalent and hydrogen bonds with the same halogen ($\angle HXH$) for the low-temperature $Cmc2_1$ phase of HF, HCl, and HBr at ambient pressure, compared with available experimental data.

		a (Å)	b (Å)	c (Å)	V (Å^3)	$d_{H\text{-}X}$ (Å)	$d_{X\text{-}X}$ (Å)	$\angle HXH$ (deg)
HF	This work	3.586	5.573	4.059	81.109	1.013	2.390	116.210
	Expt.[a]	3.310	5.220	4.260	73.605	0.951	2.503	116.603
HCl	This work	6.576	5.171	5.173	175.884	1.317	3.502	95.219
	Expt.[b]	5.825	5.053	5.373	158.147	1.250	3.688	93.516
HBr	This work	7.073	5.491	5.440	211.271	1.473	3.768	92.415
	Expt.[c]	6.068	5.377	5.590	182.398	1.401	4.008	88.430

[a]Reference 6.
[b]Reference 10.
[c]Reference 9.

pressures predicted spontaneous formation of H_2 with monatomic Br lattice at above 40 GPa, instead of the emergence of Br_2 molecules.[20]

As described above, the documented experimental studies on high-pressure behaviors of hydrogen halides were mainly limited to spectroscopic measurements due to the well-known failure of determining hydrogen positions for *in situ* x-ray diffraction measurements and the related high-pressure structures thus remain a lot of controversy. It has been a strong request to understand the physical mechanism of pressure-induced hydrogen-bond symmetrization and clarify the phase diagram of hydrogen halides at high pressures. Here we report an extensive *ab initio* study on phase transformations of solid HF, HCl, and HBr at pressures up to 200 GPa using the evolutionary algorithm for crystal-structure predictions,[21–24] and the results on HI will be presented elsewhere owing to its unique ambient-pressure structure and transformation behaviors. Our crystal-structure predictions based on the only information of chemical compositions have successfully reproduced the ambient-pressure phase of $Cmc2_1$ and following *Cmcm* phase with symmetric hydrogen bonds for all the three hydrogen halides, supporting the validity of current methodology. By further analysis of calculated results, we elucidated the physical mechanism of hydrogen-bond symmetrization at the $Cmc2_1 \rightarrow Cmcm$ transformation. At high pressures, we predicted that the symmetric hydrogen-bonded molecular phase, chain-type *Pnma* phase for HF and square-type $P\bar{1}$ phase for HCl and HBr, dominate.

II. COMPUTATIONAL METHOD AND RELIABILITY CHECK

The stable crystal structures (with the lowest Gibbs free energy) in the range of 0–200 GPa were explored by merging *ab initio* total-energy calculations and the evolutionary algorithm, as implemented in the USPEX code.[21–24] In this approach, no initial experimental information except for chemical compositions is required and thus it provides fully nonempirical crystal-structure predictions. The theoretical details of this algorithm and its successful applications in several systems have been described elsewhere.[22,25–30] The underlying free-energy calculations (reduced to enthalpy at zero temperature) and structure optimizations were performed within the framework of generalized gradient approximation[31] using the frozen core all-electron projector-augmented wave method,[32] as implemented in the VASP code.[33,34] The $1s^1$ for H and s^2p^5 for halogens were treated as valence electrons. For the size of plane-wave basis set, we used the kinetic energy and augmented charge cutoff of 520 eV and 614 eV for HF, 370 eV and 400 eV for HCl, and 375 eV and 504 eV for HBr, respectively, which were carefully checked and shown to give well converged energy and force required for the current study. All the predicted stable structures are further fully optimized at selected pressures with the energy tolerance of 10^{-4} eV, and then the enthalpies were calculated. The Brillouin zone sampling for self-consistent calculations was done using the special k-point method[35] with different converged grids for individual structures. The phonon calculations were performed and cross-checked using both the linear-response method[36] (QUANTUM-ESPRESSO code)[37] and small displacement method[38] (FROPHO code),[39] which give consistent results.

Before entering high-pressure studies, we have checked the suitability and reliability of density-functional calculations and evolutionary structure predictions for currently studied hydrogen halides at ambient pressure. The equilibrium structural parameters for low-temperature $Cmc2_1$ phase of these halides are fully optimized by total-energy minimization and compared with experimental data[6,9,10] in Table I. It can be seen that our theoretical results generally overestimate crystalline volumes for all the halides (10.0%, 11.2%, and 15.8% for HF, HCl, and HBr, respectively). This mainly originates from the known failure of standard density-functional theory on dealing with the van der Waals interactions between adjacent molecular chains in the present system. The largest discrepancy is found for the a-lattice constant, along which direction the van der Waals interactions dominate. Figure 2 presents the calculated equation of state (EOS) for the $Cmc2_1$ phase by fitting total energy vs volume data to the Murnaghan EOS.[42] As seen, apart from

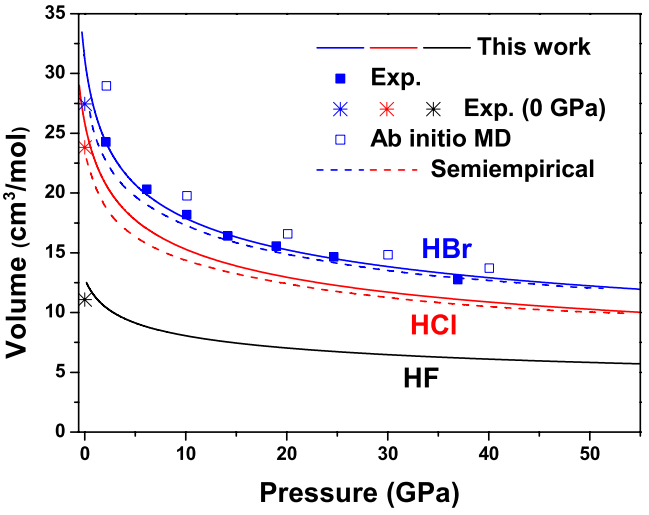

FIG. 2. (Color online) Calculated equation of state for HF, HCl, and HBr using the $Cmc2_1$ structure, by comparison with available experimental data (for HBr), Refs. 20 and 40, previous *ab initio* MD simulation (Refs. 20 and 40), and semiempirical results (Ref. 41). The experimental ambient-pressure data (Refs. 6, 9, and 10) in Table I are also shown.

the overestimation of volumes at ambient pressure as mentioned, our results on HBr are in good agreement with the available experimental data at higher pressures.[40] This is somewhat different from the earlier AIMD study,[40] which overestimates volumes in all the pressure range. From our results, it is implied that the effects of van der Waals interactions are remarkably reduced under compression. This indicates that the present standard density-functional calculations are suitable for studying higher-pressure behaviors of these systems. Turning to structure predictions, we performed variable-cell simulations with the unit cells containing two and four H*X* molecules at ambient pressure. The experimental $Cmc2_1$ phase consisting of zigzag chains (with two molecules in the primitive unit cell, see Fig. 1) is robustly reproduced as the most stable structure in both simulations for all the halides. In particular, the specific structural character such as the larger angle value of ∠H*X*H for HF (~120°) than those of HCl/Br (~90°, see Table I) is also well captured by our structure predictions. These results support the reliability of current crystal-structure predictions and give us confidence to explore high-pressure structures.

III. PHASE IV: HYDROGEN-BOND SYMMETRIZATION

The variable-cell structure prediction simulations were performed with the unit cells containing two and four molecules at 40 GPa for HF, at 50 GPa for HCl, and at 40 GPa for HBr, respectively. We found that the most stable phase for all the halides is the *Cmcm* structure (two molecules, $Z=2$ for the primitive unit cell) with symmetric hydrogen bonds. This prediction is in excellent agreement with experimental observations.[12,16–19] Further enthalpy calculations (Fig. 3) have confirmed stability of the *Cmcm* structure at above 25 GPa, 35 GPa, and 25 GPa for HF, HCl, and HBr, respectively.

In an attempt to present a more transparent picture for the hydrogen-bond symmetrization during the $Cmc2_1 \rightarrow Cmcm$ transition, we have performed structural optimizations for the $Cmc2_1$ phase upon pressure. The calculated variation in covalent bond lengths, hydrogen-bond lengths, and nearest *X*-*X* distances (the sum of former two) with pressure are depicted in Fig. 4. As seen, all halides share common features of gradual elongation of intramolecular covalent bonds and shrinkage of hydrogen bonds. This clearly indicates that under compression the covalent bonds are weakened while hydrogen bonds are strengthened, which originates from a pressure-induced charge transfer from the region of covalent bonds to hydrogen bonds (see below). Meanwhile, the *X*-*X* distance continuously decreases with pressure, which is, in fact, a more direct driving force for the change in bond lengths.[43] Signaled by two equal (covalent and hydrogen) bond lengths, the hydrogen-bond symmetrization is accomplished at about 25 GPa, 35 GPa, and 25 GPa for HF, HCl, and HBr, respectively. As expected, all the structures after the symmetrization naturally take the form of *Cmcm*. It is worth noting that the critical pressures corresponding to hydrogen-bond symmetrization almost perfectly match with those transition pressures derived from enthalpy calculations

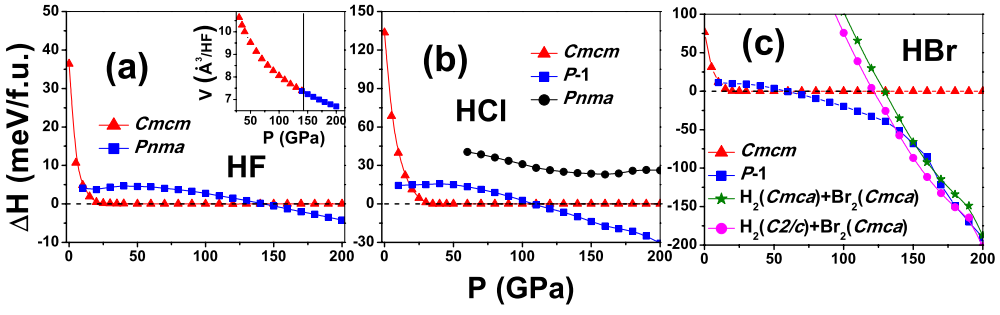

FIG. 3. (Color online) Enthalpy difference (relative to the $Cmc2_1$ phase) as a function of pressure for predicted high-pressure phases of *Cmcm*, *Pnma*, and $P\bar{1}$, as well as the dissociation into H_2+Br_2 for solid (a) HF, (b) HCl, and (c) HBr. Note that with increasing pressure, the $Cmc2_1$ phase continuously transforms to the symmetric *Cmcm* phase. We have checked validity of the *Pnma* phase for HBr and $P\bar{1}$ phase for HF, which have much higher enthalpies even compared with the $Cmc2_1$ phase and thus are not shown. The inset of (a) shows calculated EOS for *Cmcm* and *Pnma* phases of HF during the transition. It should be pointed out that in (c) the *Cmca* structure of Br_2 actually has dissociated to the monatomic phase (*Fmmm*).

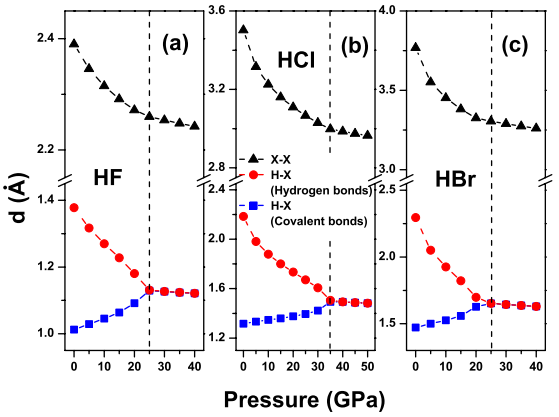

FIG. 4. (Color online) Evolution with pressure of bond lengths for covalent bonds and hydrogen bonds, and distances between nearest halogens (*X*-*X*) for (a) HF, (b) HCl, and (c) HBr, calculated with optimized $Cmc2_1$ structures starting from 0 GPa. The pressure where the hydrogen-bond symmetrization occurs is marked with a vertical dashed line.

(Fig. 3), further implying that the $Cmc2_1 \rightarrow Cmcm$ transition is originated from pressure-induced hydrogen-bond symmetrization. Since this structural transition is derived from the continuous change in structural parameters (Fig. 4), it can be characterized as the second-order nature, which is also indicated by the feature of enthalpy curves (Fig. 3) and continuous volume changes at the transformation (not shown). It should also be pointed out that the currently calculated transition pressures for HCl and HBr (~35 and 25 GPa) are evidently lower than the experimental values [51 GPa (Ref. 16) for HCl and 39 GPa (Ref. 17) for HBr]. This discrepancy might mainly originate from the neglect of temperature effect in this work since experiments were carried out at room temperature. We recall that at room temperature, HCl (Br) adopts the disordered phase I, while it needs a 19 GPa for HCl (Ref. 16) and 13 GPa for HBr (Ref. 17) to transform into the phase III ($Cmc2_1$). If we subtract these extra pressures needed for the disorder-order phase transition, the experimental transition pressures of $Cmc2_1 \rightarrow Cmcm$ are actually 32 GPa for HCl and 26 GPa for HBr, which are in good agreement with present theoretical values. Obviously future experiments carried out at low temperatures are necessary to clarify this fact. On the other hand, our calculations do not include the proper treatment on the van der Waals interactions, which might also to some extent be responsible for the discrepancy between theory and experiments. Nevertheless, it is apparent that the theoretical transition pressure of HCl is 10 GPa higher than that of HBr, which agrees with the difference of 12 GPa observed in experiments.[16,17]

To gain further insight into the origin of pressure-induced hydrogen-bond symmetrization in this system, we performed additional analysis of electron localization functions (ELFs) for HBr projected onto the chain plane (Fig. 5). As known, the topological analysis of ELFs is widely used to probe the degree of electron localization and nature of chemical bonds in molecules and solids. Specifically, ELFs=1 corresponds to an extreme localization while ELFs=0.5 reflects the behavior of homogeneous electron gas. Here, at ambient pressure we

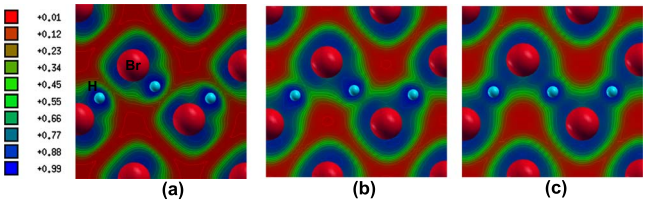

FIG. 5. (Color online) Electron localization function maps projected onto the (100) plane where the zigzag chains lie in for the $Cmc2_1$ structure of HBr at (a) 0 GPa, (b) 15 GPa, and (c) 30 GPa, respectively. Note that at 30 GPa the symmetric *Cmcm* phase occurs.

clearly see strong covalent bonds with electrons prominently localized within HBr molecules, as well as much weaker intermolecular hydrogen bonds. Upon compression, as hydrogen atoms move toward the midpoint between two Br atoms, electrons partially transfer from intramolecular to intermolecular region, which results in weakened covalent bonds and strengthened hydrogen bonds. After the transition, hydrogen bonds with two Br atoms to form strong symmetric bonds.

The underlying mechanism of hydrogen-bond symmetrization could be further understood by exploring the shape change in the potential well for hydrogens.[2] We performed calculations on this type of potential well by displacing the hydrogen atom along two neighboring halogen atoms within chains (Fig. 6). At ambient pressure a double potential well (in relation to asymmetric bonds) forms in all halides. With increasing pressure (for instance, in HBr), the double-well shape becomes shallower and shallower, and eventually disappears and emerges into a flat global single-well potential in the symmetric phase. This provides a direct and clear explanation for the occurrence of hydrogen-bond symmetrization in this system. It is worth noting that for another hydrogen bonds containing system, ice, before the formation of hydrogen-bond symmetrized phase X, the asymmetric phase VIII first transforms to a proton-disordered phase VII, where

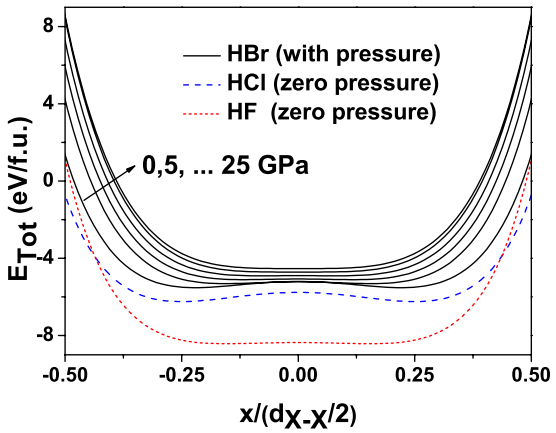

FIG. 6. (Color online) Calculated total energies for three halides at zero pressure as a function of the ratio between the displacement of hydrogen away from the midpoint of two nearest halogens (x) and half of distances between the halogens ($d_{X\text{-}X}/2$). Here, as an illustrative case, we only show the curves with pressure (0–25 GPa) for HBr.

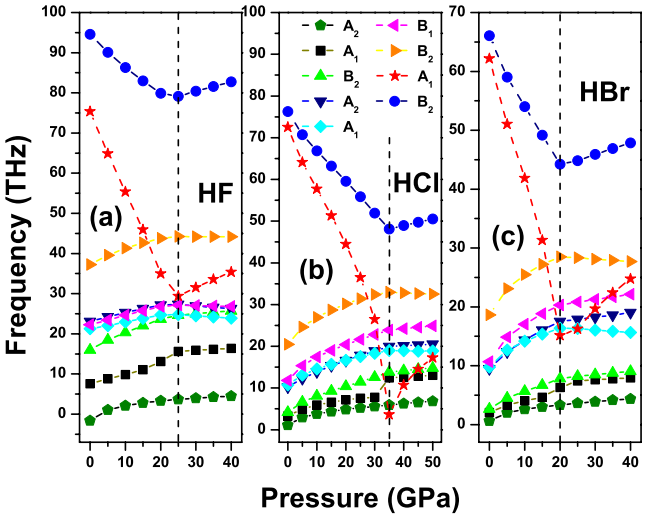

FIG. 7. (Color online) Calculated frequencies of zone-center optical phonons as a function of pressure for $Cmc2_1$ and $Cmcm$ phases in (a) HF, (b) HCl, and (c) HBr. The crossover of stretching modes denoted by the dashed line is an indication of phase transition.

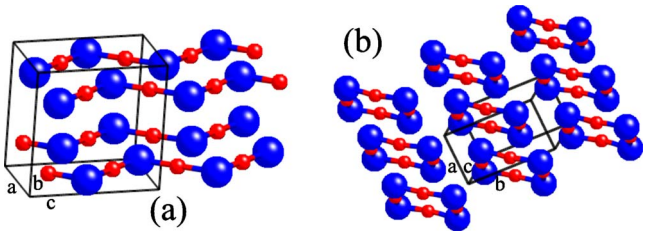

FIG. 8. (Color online) Crystal structures of the predicted high-pressure post-*Cmcm* phases: (a) the *Pnma* structure for HF and (b) the $P\bar{1}$ structure for HCl/Br. Hydrogen atoms are shown as smaller spheres and halogens as larger ones. At 160 GPa, the structural parameters for the *Pnma* structure of HF are a=3.6170 Å, b=3.5624 Å, and c=2.2079 Å, with H and F atoms occupying 4c (0.4244, 1/4, 0.7560) and 4c (0.6728, 1/4, 0.4844) positions, respectively. The structural parameters for the $P\bar{1}$ structure of HCl at 150 GPa are a=2.5841 Å, b=4.2279 Å, c=4.51 Å, α=88.87°, β=89.59°, and γ=87.24°, with two inequivalent H atoms occupying 2i (0.7499, 0.2638, 0.0889) and 2i (0.1955, 0.9961, 0.2903) sites and two inequivalent Cl atoms sitting at 2i (0.4602, 0.2671, 0.3605) and 2i (0.0885, 0.2513, 0.8430).

protons distribute in two minimums of the double-well potential with equal probability due to effects of translational proton tunneling and zero-point fluctuations.[2,44] Turning to HBr, in the pressure region approaching hydrogen-bond symmetrization, two minimums of the double-well potential get closer and the height of barrier separating two double wells becomes very low. One therefore suggests that this could increase the probability of related proton tunneling. Thus, it can be conjectured that proton-disordered behaviors might also occur before completed hydrogen-bond symmetrization in these hydrogen halides, though there is no such disordered phase reported so far. Especially, the proton disorder might even exist at low pressures in HF by noticing its quite small barrier height at ambient pressure.

We then calculated the pressure dependence of optical phonons at zone center for three halides, as shown in Fig. 7. Group-theory analysis suggests that all the nine optical modes ($3A_1+2A_2+1B_1+3B_2$) are Raman active, of which those modes of A_1, B_1, and B_2 are also infrared active. As seen, most of phonons increase frequencies with pressure except for two high-frequency stretching B_2 (antisymmetric, labeled as blue circles) and A_1 (symmetric, red stars) modes contributed from hydrogen, which remarkably soften under compression. These behaviors are consistent with experimental observations.[16–19] The softening of these stretching modes is originated from the weakening of covalent bonds with increasing pressures as directly supported in Fig. 5. After transformation into the symmetric *Cmcm* phase, the stretching modes harden gradually as the result of pressure-induced strengthened symmetric bonds. The emergence of hydrogen-bond symmetrization can be well characterized by the crossover of stretching modes in two phases. In experiments, no stretching mode was observed for the symmetric *Cmcm* phase,[16–19] which might be attributed to small scattering cross-sections. It is important to point out that the symmetric stretching A_1 mode never softens to zero frequency before the formation of bond symmetric phase. This is somehow in contrast to usual expectation for the hydrogen-bond symmetrization, but has been strongly supported by the fact that the actual transition pressure observed in experiments is lower than the extrapolation pressure to zero frequency for this stretching mode.[16–19] In addition, one can also observe that the low-lying translational A_1 mode (labeled as black squares) shows a clear discontinuity at the transformation, which is in good agreement with experimental observations (e.g., Fig. 3 in Ref. 18 and Fig. 4 in Ref. 17).

IV. PHASE V AT HIGH PRESSURES

To further explore the post-*Cmcm* high-pressure phases, we performed variable-cell structural predictions for HF at 40, 80, 120, 160, and 200 GPa, for HCl at 50, 100, 150, and 200 GPa, and for HBr at 40, 80, and 120 GPa containing two, four, and eight molecules, respectively. It was found that the *Cmcm* phase remains stable up to 120 GPa for HF, 100 GPa for HCl, and 40 GPa for HBr. At 160 and 200 GPa, simulations for HF predict an orthorhombic *Pnma* structure [Z=4, see Fig. 8(a)] to be most stable. This structure also consists of similar planar zigzag chains with symmetric hydrogen bonds as in the *Cmcm* phase. However, the spatial arrangement of these zigzag chains is revised remarkably. In particular, the distances between neighbor chains within the same plane reduce to be almost half while the distances between two planes expand to be twice of that in the *Cmcm* phase. Thus this dramatic structural rearrangement does not obviously alter volumes. As shown in the inset of Fig. 3(a), the volume change at the transition of *Cmcm*→*Pnma* is nearly continuous. The stability field of *Pnma* phase for HF was calculated to be above 143 GPa as determined from the enthalpy curves [Fig. 3(a)].

For HCl at 150 and 200 GPa, and HBr at 80 and 120 GPa, our structural predictions revealed the triclinic $P\bar{1}$ structure

[Fig. 8(b)] as the most stable one. This structure contains four molecules in the unit cell and only possesses the space-inversion symmetry. In contrast to HF, the zigzag chains in HCl and HBr collapse at high pressures with the formation of intriguing distorted squares, where the halogen atoms are connected by symmetric hydrogen bonds. It is noted that our predicted high-pressure $P\bar{1}$ phase for HCl and HBr resembles in some aspects the low-temperature ordered $P\bar{1}$ phase of HI at ambient pressure,[9] where HI molecules are also arranged in the form of distorted squares. Differently, the distorted squares in HI are connected by asymmetric hydrogen bonds, and here the predicted $P\bar{1}$ structure does not contain obvious layers consisting of squares. Our enthalpy calculations [Figs. 3(b) and 3(c)] confirmed the stability of $P\bar{1}$ phase in HCl and HBr at above 108 GPa and 59 GPa, respectively. To explore the possibility of molecular dissociations (to Br_2) proposed earlier in HBr,[16,17] we calculated the enthalpy for decomposition into H_2+Br_2, using the *Cmca* structure of solid Br_2,[45] $C2/c$ (Ref. 46) and *Cmca* (Ref. 47) structures of solid H_2, as shown in Fig. 3(c). It can be clearly seen that below 100 GPa the predicted high-pressure phases (including the *Cmcm* phase) are reliably stable (more than 50 meV lower) against decomposition, though the energy of decomposition decreases dramatically with increasing pressures. For pure hydrogen, it is known that the quantum effects such as zero-point energies play a notable role in determining structural instability. If one includes zero-point energies, this will enhance the total energy of H_2+Br_2, further against decomposition. Above 120 GPa, the fast-decreasing enthalpies of decomposition become comparable with that of the $P\bar{1}$ phase, implying possible occurrence of molecular dissociations. In such high-pressure range, solid bromine is predicted to adopt monatomic phase rather than Br_2 molecule form,[48,49] as also indicated in our calculations where the *Cmca* Br_2 has actually transferred to the monatomic *Fmmm* phase (intramolecular and intermolecular distances become indistinguishable) in the high-pressure range shown for decomposition. This prediction is qualitatively consistent with previous AIMD study.[20] Similar decomposition calculations were also performed for HCl and in contrast we obtained quite stable status for high-pressure phases. Particularly its decomposition energy is more than 500 meV/f.u. higher than the *Cmcm* phase up to 200 GPa, though the corresponding curve also shows decreasing trend with pressure.

The exploration of underlying mechanism for the broken down of chain-type structure and formation of planar square unit in HCl and HBr at high pressures seems challenging, but extremely interesting. From Table I, as mentioned the bond angle within zigzag chains in HCl and HBr is ~90°, much smaller than that in HF (~120°), which might originate from the stronger hydrogen bondings in HF and larger dipole moment of the HF molecule. As a result, the stronger interactions between neighboring chains for HCl and HBr are expected at high pressures, which might lead to the reconstruction from chain to square units. Clearly much effort is needed to fully understand this intriguing mechanism. An essential requirement for the stable structure is lattice dynamical stability.[50] We thus calculated the phonon dispersions for our newly predicted *Pnma* and $P\bar{1}$ structures for HF and HCl/HBr, as shown in Fig. 9. It is quite clear that both *Pnma* and $P\bar{1}$ phases are dynamically stable evidenced by absence of any imaginary phonons in the whole Brillouin zone. For the $P\bar{1}$ phase of HCl/Br, because of the larger difference in atomic masses, the phonon spectrum has been unambiguously divided into three parts: high-frequency modes from hydrogen stretching vibrations, middle region from hydrogen wagging modes and low-frequency part mainly contributed by halogen's vibrations and motion of lattice. Turning to the *Pnma* phase of HF [Fig. 9(a)], these partitions are not so obvious due to relatively similar atomic

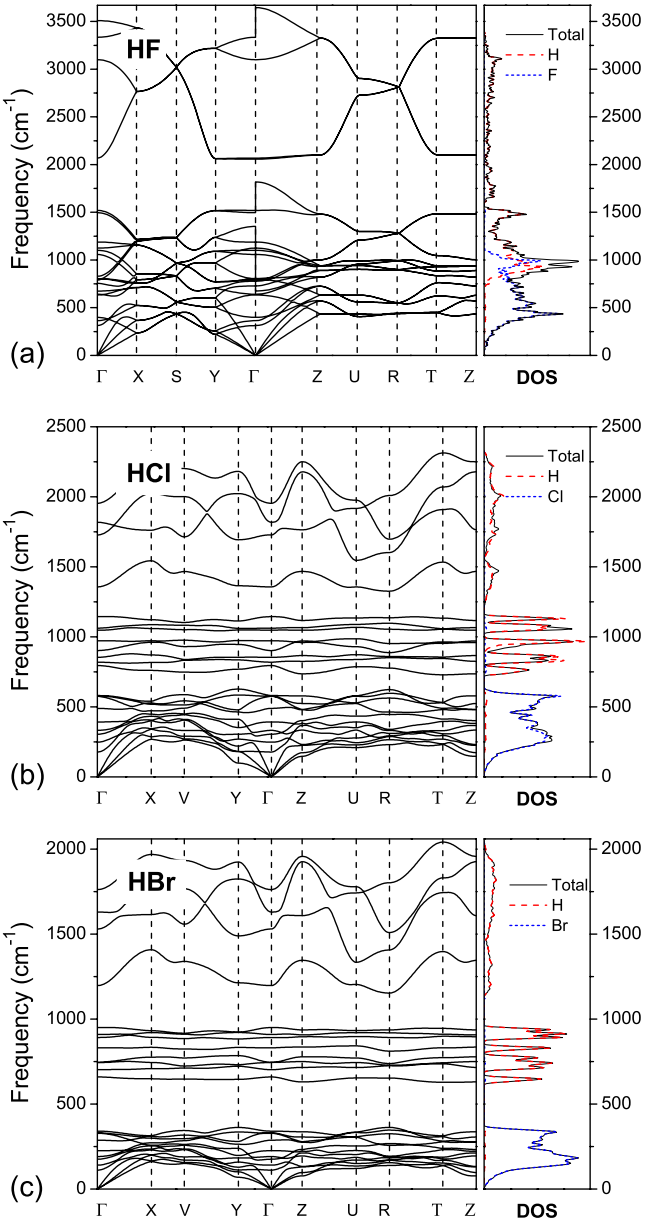

FIG. 9. (Color online) Calculated phonon dispersion curves as well as phonon density of states (DOS) and its projection onto individual atom for the newly predicted phase of HF [(a) the *Pnma* structure] at 180 GPa, HCl [(b) the $P\bar{1}$ structure] at 130 GPa, and HBr [(c) the $P\bar{1}$ structure] at 80 GPa.

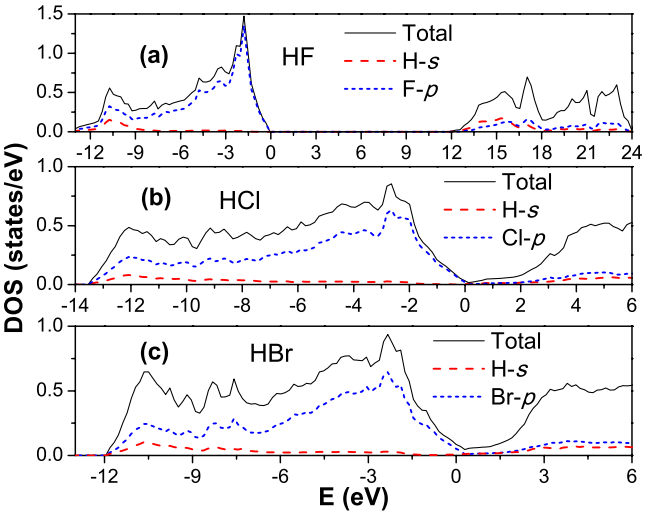

FIG. 10. (Color online) Electronic DOS and projections onto atomic orbitals for the predicted phase of HF at 180 GPa [(a) the *Pnma* structure], HCl at 130 GPa [(b) the $P\bar{1}$ structure], and HBr at 80 GPa [(c) the $P\bar{1}$ structure]. For HF, the zero energy is set as the maximum of valence bands. For HCl and HBr, the Fermi level is set as zero energy.

masses and the modes' overlapping occurs. As an insulator with quite large band gap (see below), there appears large LO-TO splittings along the Y-Γ-Z direction.

Finally, we examined electronic structures for the predicted phase V as shown in Fig. 10. For HCl and HBr, we can see typically semimetallic behaviors as the result of band overlapping at high pressures. The exploration of superconductivity at high pressures for these two materials is thus of interest, but out of scope of this work. However, it is needed to be addressed that the electrons contributed to Fermi surface are mainly from Cl/Br *p* states. This does not share the notion in group IV hydrides at high pressures where H *s* states give quite important contribution to Fermi surface.[4,51] Instead, the *Pnma* phase of HF still exhibits a large band gap (above 10 eV) in the pressure range investigated. Considering that the band gap is usually underestimated by normal density-functional calculations, extremely ultrahigh pressure would be needed to accomplish metallic HF in experiments.

V. SUMMARY AND CONCLUSIONS

To conclude, we have explored high-pressure phase transitions of solid HF, HCl, and HBr using the evolutionary algorithm combining first-principles calculations in crystal-structure predictions. First, the ambient-pressure phase of $Cmc2_1$ structure consisting of planar zigzag chains was well reproduced by structure searches for all the compounds. With increasing pressure, we confirmed the experimentally observed phase IV (the *Cmcm* structure) with symmetric hydrogen bonds, based on both directly structural optimizations starting from the $Cmc2_1$ phase and comprehensive structure predictions with the only known information of chemical compositions. We then provided a deep insight into the underlying mechanism of hydrogen-bond symmetrization at the phase transition, by analysis of electron localization functions, related potential wells, and zone-center phonons with increasing pressure. Especially, it was found that the high-frequency symmetric A_1 stretching mode softens dramatically with pressure and shows clear crossover at the transition, rather than decreases to zero frequency as usual expectation for hydrogen-bond symmetrization.

In contrast to the common structures of $Cmc2_1$ and *Cmcm* for these halides at low pressures, the predicted stable post-*Cmcm* phase at high pressures is entirely different between HF and HCl (Br). Owing to strong symmetric hydrogen bonds, HF transfers to an orthorhombic *Pnma* structure at above 143 GPa, where zigzag chains in the *Cmcm* phase are preserved but arranged in a different way. For HCl and HBr, the intriguing planar squares with breakdown of the zigzag chains were formed under strong compression. The new structure takes the triclinic $P\bar{1}$ type and is stable above 108 GPa for HCl and 59 GPa for HBr. Interestingly, the predicted $P\bar{1}$ structure in some aspects resembles the ambient phase of HI. Moreover, we have ruled out the earlier proposed decomposition of HBr into H_2+Br_2 below 100 GPa, judged by much lower energy of the predicted $P\bar{1}$ phase than decomposition. At high pressures above 120 GPa, it is predicted based on our results that the decomposition to monatomic Br and solid H_2 might occur. The newly predicted post-*Cmcm* phases for these halides show robust dynamical stability evidenced by absence of any imaginary phonon modes. Electronic-structure calculations indicate that the $P\bar{1}$ phase of HCl and HBr show weak metallic features while the *Pnma* phase of HF exhibits large band gap within the pressure range investigated. We point out the search on the superconductivity of HCl and HBr is of interest for both theoretical simulations and experiments.

ACKNOWLEDGMENTS

We are thankful for financial support from the National Natural Science Foundation of China (NSFC) under Grants No. 10874054 and 10910263, the China 973 Program under Grant No. 2005CB724400, and the research fund for Excellent young scientist in Jilin University (Grant No. 200905003).

*Author to whom correspondence should be addressed; mym@jlu.edu.cn

[1] A. F. Goncharov, V. V. Struzhkin, M. S. Somayazulu, R. J. Hemley, and H. K. Mao, Science **273**, 218 (1996).
[2] M. Benoit, D. Marx, and M. Parrinello, Nature (London) **392**, 258 (1998).
[3] P. Loubeyre, R. Letoullec, E. Wolanin, M. Hanfland, and D. Hausermann, Nature (London) **397**, 503 (1999).
[4] N. W. Ashcroft, Phys. Rev. Lett. **92**, 187002 (2004).
[5] J. van Straaten and I. F. Silvera, Phys. Rev. Lett. **57**, 766 (1986).
[6] M. W. Johnson, E. Sandor, and E. Arzi, Acta Crystallogr., Sect. B: Struct. Crystallogr. Cryst. Chem. **31**, 1998 (1975).
[7] J. E. Vesel and B. H. Torrie, Can. J. Phys. **55**, 592 (1977).
[8] A. Anderson, B. H. Torrie, and W. S. Tse, J. Raman Spectrosc. **10**, 148 (1981).
[9] A. Ikram, B. H. Torrie, and B. M. Powell, Mol. Phys. **79**, 1037 (1993).
[10] E. Sándor and R. F. C. Farrow, Nature (London) **213**, 171 (1967).
[11] W. Y. Zeng, Y. Z. Mao, and A. Anderson, J. Raman Spectrosc. **30**, 995 (1999).
[12] D. A. Pinnick, A. I. Katz, and R. C. Hanson, Phys. Rev. B **39**, 8677 (1989).
[13] A. Polian and M. Grimsditch, Phys. Rev. Lett. **52**, 1312 (1984).
[14] S. A. Lee, D. A. Pinnick, S. M. Lindsay, and R. C. Hanson, Phys. Rev. B **34**, 2799 (1986).
[15] T. Kume, T. Tsuji, S. Sasaki, and H. Shimizu, Phys. Rev. B **58**, 8149 (1998).
[16] K. Aoki, E. Katoh, H. Yamawaki, M. Sakashita, and H. Fujihisa, Physica B **265**, 83 (1999).
[17] E. Katoh, H. Yamawaki, H. Fujihisa, M. Sakashita, and K. Aoki, Phys. Rev. B **59**, 11244 (1999).
[18] E. Katoh, H. Yamawaki, H. Fujihisa, M. Sakashita, and K. Aoki, Phys. Rev. B **61**, 119 (2000).
[19] P. G. Johannsen, W. Helle, and W. B. Holzapfel, J. Phys. (Paris), Colloq. **45**, C8 (1984).
[20] T. Ikeda, M. Sprik, K. Terakura, and M. Parrinello, J. Chem. Phys. **111**, 1595 (1999).
[21] A. R. Oganov, C. W. Glass, and S. Ono, Earth Planet. Sci. Lett. **241**, 95 (2006).
[22] A. R. Oganov and C. W. Glass, J. Chem. Phys. **124**, 244704 (2006).
[23] C. W. Glass, A. R. Oganov, and N. Hansen, Comput. Phys. Commun. **175**, 713 (2006).
[24] A. R. Oganov and C. W. Glass, J. Phys.: Condens. Matter **20**, 064210 (2008).
[25] Y. Ma, A. R. Oganov, Z. Li, Y. Xie, and J. Kotakoski, Phys. Rev. Lett. **102**, 065501 (2009).
[26] Y. Ma, A. R. Oganov, and C. W. Glass, Phys. Rev. B **76**, 064101 (2007).
[27] G. Gao, A. R. Oganov, A. Bergara, M. Martinez-Canales, T. Cui, T. Iitaka, Y. Ma, and G. Zou, Phys. Rev. Lett. **101**, 107002 (2008).
[28] Q. Li, Y. Ma, A. R. Oganov, H. Wang, H. Wang, Y. Xu, T. Cui, H. K. Mao, and G. Zou, Phys. Rev. Lett. **102**, 175506 (2009).
[29] Y. Ma, M. Eremets, A. R. Oganov, Y. Xie, I. Trojan, S. Medvedev, A. O. Lyakhov, M. Valle, and V. Prakapenka, Nature (London) **458**, 182 (2009).
[30] A. R. Oganov, J. Chen, C. Gatti, Y. Ma, C. W. Glass, Z. Liu, T. Yu, O. O. Kurakevych, and V. L. Solozhenko, Nature (London) **457**, 863 (2009).
[31] J. P. Perdew, K. Burke, and M. Ernzerhof, Phys. Rev. Lett. **77**, 3865 (1996).
[32] G. Kresse and D. Joubert, Phys. Rev. B **59**, 1758 (1999).
[33] G. Kresse and J. Furthmuller, Phys. Rev. B **54**, 11169 (1996).
[34] G. Kresse and J. Furthmuller, Comput. Mater. Sci. **6**, 15 (1996).
[35] H. J. Monkhorst and J. D. Pack, Phys. Rev. B **13**, 5188 (1976).
[36] S. Baroni, S. de Gironcoli, A. Dal Corso, and P. Giannozzi, Rev. Mod. Phys. **73**, 515 (2001).
[37] P. Giannozzi *et al.*, J. Phys.: Condens. Matter **21**, 395502 (2009).
[38] K. Parlinski, Z-. Q. Li, and Y. Kawazoe, Phys. Rev. Lett. **78**, 4063 (1997).
[39] A. Togo, F. Oba, and I. Tanaka, Phys. Rev. B **78**, 134106 (2008).
[40] T. Ikeda, M. Sprik, K. Terakura, and M. Parrinello, Phys. Rev. Lett. **81**, 4416 (1998).
[41] J. van Straaten and I. F. Silvera, Phys. Rev. B **36**, 9301 (1987).
[42] F. D. Murnaghan and A. J. Math, Proc. Natl. Acad. Sci. U.S.A. **30**, 244 (1944).
[43] R. W. Jansen, R. Bertoncini, D. A. Pinnick, A. I. Katz, R. C. Hanson, O. F. Sankey, and M. O'Keeffe, Phys. Rev. B **35**, 9830 (1987).
[44] M. Bernasconi, P. L. Silvestrelli, and M. Parrinello, Phys. Rev. Lett. **81**, 1235 (1998).
[45] B. M. Powell, K. M. Heal, and B. H. Torrie, Mol. Phys. **53**, 929 (1984).
[46] C. J. Pickard and R. J. Needs, Nat. Phys. **3**, 473 (2007).
[47] K. A. Johnson and N. W. Ashcroft, Nature (London) **403**, 632 (2000).
[48] T. Kume, T. Hiraoka, Y. Ohya, S. Sasaki, and H. Shimizu, Phys. Rev. Lett. **94**, 065506 (2005).
[49] D. Duan, Y. Liu, Y. Ma, Z. Liu, T. Cui, B. Liu, and G. Zou, Phys. Rev. B **76**, 104113 (2007).
[50] M. Born and K. Huang, *Dynamical Theory of Crystal Lattices* (Oxford University Press, USA, 1988).
[51] J. S. Tse, Y. Yao, and K. Tanaka, Phys. Rev. Lett. **98**, 117004 (2007).